VIII International Conference on Computational Methods in Marine Engineering
MARINE 2019
R. Bensow and J. Ringsberg (Eds)

NUMERICAL MODELING OF CONTACT DISCONTINUITIES IN TWO-PHASE FLOW

RONALD A. REMMERSWAAL[*] AND ARTHUR E. P. VELDMAN[†]

[*,†]Bernoulli Institute for Mathematics, Computer Science and Artificial Intelligence
University of Groningen, The Netherlands
[*]r.a.remmerswaal@rug.nl [†]a.e.p.veldman@rug.nl

Key words: two-phase flow, contact discontinuity, Ghost Fluid Method, Cut Cell Method

Abstract. For convection dominated two-phase flow, velocity components tangential to the interface can become discontinuous when interface boundary layers are numerically underresolved. When sharp interface tracking methods are used it is essential that such discontinuities are captured in an equally sharp way.

In this paper we propose to model the velocity component tangential to the interface as discontinuous using an appropriate interface jump condition on the normal component of the pressure gradient. We achieve this numerically using a novel combination of a Multi-dimensional Ghost Fluid Method for the gradient and the Cut Cell Method for the divergence operator. The resulting model is able to accurately and sharply capture discontinuities at large density ratios.

The model is applied to an inviscid dam-break problem. Here we observe that our proposed model accurately captures the shear layer at the interface with the tangential velocity discontinuity.

In future work we will apply this discretization approach to the modeling of viscous two-phase sloshing problems with LNG and its compressible vapour, with a particular interest in studying the development of free surface instabilities.

1 Introduction

Sloshing of fluids in a container is a complex physical phenomena which is present in many engineering problems. For instance the transport of Liquefied Natural Gas (LNG) in LNG carriers. In particular the role of free surface instabilities in measured impact pressures during breaking wave impacts, which may occur during sloshing, is not well understood [2]. Numerical modeling can facilitate this understanding.

The numerical modeling of two-phase flow involves dealing with a multitude of jumps (discontinuities) of fluid properties across the interface separating the fluids. Additional challenges arise when shear layers develop at the fluid-fluid interface, resulting in an interface boundary layer. When such an interface boundary layer is underresolved this can result in unphysical

interaction between the two fluids at the interface. Numerically such an underresolved interface boundary layer effectively results in a velocity field which has a (contact) discontinuity in the tangential direction. We therefore propose to model the underresolved velocity field as being discontinuous in the direction tangential to the interface. As a starting point we consider inviscid two-phase flow modeled by the Euler equations.

In this paper we explore the numerical modeling, in a Finite Volume setting, of contact discontinuities for incompressible and inviscid two-phase flow. To this end we describe the governing equations in Section 2, followed by our proposed discretization at the interface in Section 3. In Section 4 we demonstrate the accuracy of our discretization when applied to a Poisson problem as well as a time-dependent Euler problem in which we model a dam-break. Concluding remarks are made in Section 5.

For simplicity in notation we consider a two-dimensional setting.

2 Mathematical model

Here we briefly describe the underlying mathematical model we use, which are the incompressible Euler equations for each of the two phases $\pi = l, g$ (liquid and gas).

2.1 Primary equations

The primary equations describe the conservation of mass and momentum in each of the phases in an arbitrary control volume $\omega = \omega^l \cup \omega^g$

$$\frac{d}{dt}\int_{\omega^\pi} \rho^\pi \; dV + \int_{\partial\omega^\pi \setminus I} \rho^\pi u_\eta^\pi \; dS = 0 \tag{1}$$

$$\frac{d}{dt}\int_{\omega^\pi} \rho^\pi \mathbf{u}^\pi \; dV + \int_{\partial\omega^\pi \setminus I} \rho^\pi \mathbf{u}^\pi u_\eta^\pi \; dS = -\int_{\partial\omega^\pi} (p^\pi - \rho^\pi \mathbf{g}\cdot\mathbf{x})\eta \; dS, \tag{2}$$

where η denotes the face normal, u_η^π the face normal velocity component, p^π the pressure, $\mathbf{g}$ the gravitational acceleration and ρ^π the density per phase. We consider incompressible flow for which the mass conservation equations result in a volume constraint on the evolution of the interface

$$\frac{d}{dt}|\omega^l| + \int_{\partial\omega^l \setminus I} u_\eta^l \; dS = 0, \tag{3}$$

where $|\omega^\pi|$ denotes the volume of ω^π.

The influence of surface tension is of interest in our application and we therefore include it via Laplace's law

$$-[\![p]\!] = \sigma\kappa. \tag{4}$$

Here κ denotes the interface mean curvature and $[\![\varphi]\!]$ denotes jump of some flow variable φ

$$[\![\varphi]\!] := \varphi^g - \varphi^l. \tag{5}$$

We assume immiscible fluids without phase change, and therefore

$$[\![u_\eta]\!] = \eta \cdot (\mathbf{u}^g - \mathbf{u}^l) = 0. \tag{6}$$

Together with appropriate boundary conditions on $\mathbf{u}^\pi$ and a contact angle boundary condition on κ this results in a closed system of equations. Note that this model does not impose any smoothness on the tangential velocity component $u_\tau = \tau \cdot \mathbf{u}$, where τ denotes the interface tangent.

2.2 The pressure Poisson problem

Addition of the mass conservation equations, when divided by their respective densities, yields

$$\int_{\partial\omega} u_\eta \; dS = \int_{\partial\omega^l \setminus I} u_\eta^l \; dS + \int_{\partial\omega^g \setminus I} u_\eta^g \; dS = 0, \tag{7}$$

thus showing that the mixture velocity field is divergence free. Taking the time derivative of the divergence constraint, substituting the momentum equation and using $[\![u_\eta]\!] = 0$, yields an equation for the pressure

$$\int_{\partial\omega} \frac{1}{\rho} \partial_\eta p \; dS = -\int_{\partial\omega} \eta \cdot (\mathbf{u} \cdot \nabla)\mathbf{u} \; dS. \tag{8}$$

We supplement the aforementioned equation with Laplace's law (4), an homogeneous Neumann boundary condition on the pressure and the following jump condition on the normal derivative of the pressure gradient

$$\left[\!\!\left[\frac{1}{\rho} \partial_\eta p \right]\!\!\right] = -\left[\!\!\left[\eta \cdot \frac{D\mathbf{u}}{Dt} \right]\!\!\right], \tag{9}$$

which follows directly from the strong form of the Euler equations. The latter condition (9) is necessary for having a well-posed coupled Poisson problem.

3 Numerical model

We consider a staggered variable arrangement (Arakawa C grid) on a rectilinear grid. The grid cells are denoted by the set $\mathcal{C}$, with faces $\mathcal{F}(c)$ for $c \in \mathcal{C}$. The set of all faces is denoted by $\mathcal{F}$. A subset of the faces are cut by the interface $I(t) \subset \Omega$, we denote this time-dependent set by $\mathcal{F}_I$. Every interface face is split into its liquid and gaseous part $f = f^g \cup f^l$. This leads to the definition of $\hat{\mathcal{F}}^\pi$ containing all the (possibly cut) faces which are entirely contained in the π-phase. Moreover let $\hat{\mathcal{F}} = \hat{\mathcal{F}}^l \cup \hat{\mathcal{F}}^g$, see Figure 1.

The space of functions defined on $\mathcal{C}$ is denoted by C^h, with e.g. $p \in C^h : c \mapsto p_c \approx p(\mathbf{x}_c)$, where $\mathbf{x}_c$ is the center of cell c. Similarly we have the function space F^h, where the approximations are located at $\mathbf{x}_f$, the center of the face f. We denote by η_f the normal of the face f.The function $\alpha : \mathcal{C} \times \mathcal{F} \to \{1, -1\}$ encodes the orientation of the face normals such that $\alpha_{c,f}\eta_f$ points out of cell c.

3.1 Interface advection

The interface is represented using the volume fraction field $\tilde{\chi} = |c^l|/|c| \in C^h$ as per the Volume-of-Fluid method. Advection of the interface is performed using the Lagrangian-Eulerian Advection Scheme (LEAS) [9].

3.2 Momentum equations

In the interior of each of the phases the momentum equations are discretized using the symmetry-preserving finite-volume discretization by Verstappen and Veldman [8]. Near the interface we choose to discretize the momentum equations in strong form, thereby sacrificing exact momentum conservation at the interface but alleviating difficulties faced with having arbitrarily small cells $|c^\pi|(t)$ and non-smooth in time face areas $|f^\pi|(t)$. At the interface we use a first-order upwind convection scheme *per phase*, which relies on constant extrapolation of velocities.

The time integration is performed under a CFL constraint of 0.5 using a second-order accurate explicit method, followed by a pressure correction step

$$\frac{u_f^* - u_f^{(n)}}{\Delta t} = R\left(\frac{3}{2}u_f^{(n)} - \frac{1}{2}u_f^{(n-1)}\right)_f, \quad u_f^{(n+1)} = u_f^* - \frac{\Delta t}{\rho}(Gp)_f, \quad \forall f \in \hat{\mathcal{F}}. \tag{10}$$

Here R denotes the convection and gravity terms, and $G : C^h \to \hat{F}^h$ is the gradient operator.

3.3 Pressure Poisson problem

The solution of the Poisson problem plays a central role in the numerical model, since this is where the two phases are implicitly coupled. The gradient of the resulting pressure is used to make the mixture velocity field divergence free and it is therefore important that the Laplace operator can be decomposed in a divergence $\bar{D} : \hat{F}^h \to C^h$ and a gradient G.

Given $\bar{D}$ and G we may write the Poisson problem as (for notational convenience we let $\Delta t = 1$)

$$\bar{D}\left(\frac{1}{\rho}Gp\right)_c = \bar{D}\,(u^*)_c, \quad \forall c \in \mathcal{C} \tag{11}$$

where the gradient operator G contains the value jump due to surface tension as well as the jump in the normal derivative. We will now precisely define the divergence $\bar{D}$ and the gradient G.

3.3.1 Divergence operator

At the interface our velocity field is discontinuous, and therefore the divergence operator needs to be modified. A finite difference approach such as the Ghost Fluid Method (GFM) [4] will result in an incompatible discretization of the Poisson problem

$$\exists u \in \hat{F}_0^h \quad \text{s.t.} \quad \sum_{c\in\mathcal{C}} \bar{D}\,(u)_c \neq 0, \tag{12}$$

where $\hat{F}_0^h$ is the set of velocity fields which vanish at the boundary. A consequence of this incompatibility is that the resulting linear system of equations, resulting from the pressure Poisson equation, has no solution.

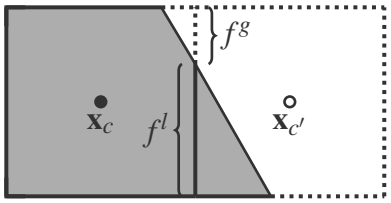

Figure 1: Illustration of the CCM. Each face is split into its liquid and gaseous part $f = f^l \cup f^g$. Shaded region corresponds to the liquid parts c^l, c'^l. Solid nodes correspond to the liquid phase and open nodes to the gas phase.

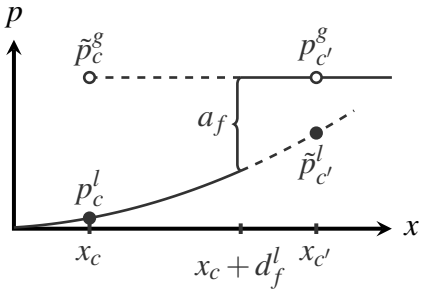

Figure 2: Illustration of the GFM. The pressure values denoted by $\tilde{p}$ are 'ghost' pressures and not actually part of the solution.

A finite-volume approach however naturally preserves the flux cancellation property which a divergence operator should satisfy, and therefore we propose to use the cut-cell method [6] for discretization of the divergence operator. To this end we define the face apertures $A_f \in F^h$ (computed from the PLIC reconstruction) as the fraction of the face $f \in \mathcal{F}$ contained in the reference fluid l, so $A_f = |f^l|/|f|$. This results in the following divergence operator

$$|c|\bar{D}(u)_c = \sum_{f \in \mathcal{F}(c)} \alpha_{c,f} |f| \bar{u}_f, \tag{13}$$

where we define the mixture velocity $\bar{u}_f = A^f u_f^l + (1 - A^f) u_f^g$. See also Figure 1. This divergence operator satisfies the discrete equivalent to Gauss's theorem exactly, and therefore the term in (12) vanishes exactly for all $u \in \hat{F}_0^h$.

3.3.2 The gradient operator

In the interior of the phases we define the gradient G as the standard finite difference operator

$$(Gp)_f = -\sum_{c \in \mathcal{C}(f)} \alpha_{c,f} \frac{p_c}{h_f}, \tag{14}$$

where h_f is the distance between the nodes $\mathbf{x}_c, \mathbf{x}_{c'}$. Near the interface the gradient needs modification to sharply capture the imposed jumps.

The Ghost Fluid Method

We consider a finite-difference approximation for the gradient at a face $f \in \mathcal{F}_I$ near the interface. The pressure $p \in C^h$ is defined point-wise according to the liquid indicator $\chi \in C^h$

$$\chi_c = \begin{cases} 1 & \text{if } \mathbf{x}_c \in \Omega^l \\ 0 & \text{if } \mathbf{x}_c \in \Omega^g \end{cases}. \tag{15}$$

Consider a face f which connects two nodes $\mathcal{C}(f) = \{c, c'\}$ from different phases (so $\chi_c \neq \chi_{c'}$). Hence we know the liquid pressure p_c^l on one side of the face and the gas pressure $p_{c'}^g$ on the other side of the face. Moreover we are given the value jump[1] $a_f = -\sigma\kappa_f$ and gradient jump b_f. The unkown scaled gradients are denoted by g_f^π. See also Figure 2.

The scaled mixture gradients, as per the Ghost Fluid Method [4], are then given by

$$\bar{g}_f = \frac{1}{\bar{\rho}_f}(\bar{G}p)_f = \frac{1}{\bar{\rho}_f}(Gp)_f + \frac{\delta_f a_f}{\bar{\rho}_f h_f} - b_f \frac{\hat{\rho}_f}{\bar{\rho}_f}, \tag{16}$$

where $\bar{\rho}_f, \hat{\rho}_f$ are average densities depending on the face aperture A_f and the distance to the interface. The difference between the liquid indicators at opposite sides of the face f is denoted by $\delta_f = h_f(G\chi)_f \in \{-1, 0, 1\}$. We recognize contributions from the standard finite difference operator, the pressure value jump and the pressure gradient jump respectively. If the value jump a_f is known at second order accuracy, it follows that the resulting gradient will be at most first order accurate in h_f.

One-dimensional GFM

From the discussion in Section 2.2 we know that we should not impose a jump on the full pressure gradient, but rather only on the component normal to the interface. In Liu et al. [4] it is assumed that the jump component tangential to the interface vanishes, resulting in

$$b_f = \alpha_{i_f,f} \left[\!\left[u_\eta^* \right]\!\right], \tag{17}$$

where $\alpha_{i_f,f} = \eta_{i_f} \cdot \eta_f$ is the face normal component of the interface normal η_{i_f}. We refer to this approach as the 'one-dimensional' GFM (1d-GFM).

Multi-dimensional GFM

Whenever the interface is not aligned with the face f (hence $|\alpha_{i_f,f}| \neq 1$), the 1d-GFM is inconsistent. We propose to replace (17) by a formula which consistently imposes the normal derivative jump condition on the gradient (9). Note that (9) involves the dot product of the full gradient with the interface normal, and therefore interpolation to the face f of interface tangential pressure derivatives will be required.

The interface configuration, defined by the indicator χ as well as the face apertures $A \in F^h$, defines two types of interface faces where the gradient will be modified:

- If a face f connects two nodes $\mathcal{C}(f) = \{c, c'\}$ from different phases (so $\chi_c \neq \chi_{c'}$) then we call this an interface normal face. See also Figure 3. The set of all interface normal faces is denoted by $\mathcal{F}_{I_\eta}$.

- On the other hand, if a face f connects two nodes from the same phase, but with a non-trivial aperture (so $A_f \notin \{0, 1\}$) then we call this an interface tangential face. See also Figure 4. The set of all interface tangential faces is denoted by $\mathcal{F}_{I_\tau}$.

[1] The curvature κ_f is interpolated from a cell-based curvature $\kappa \in C^h$ which in turn is computed using local height functions, which are generalized [5] if needed.

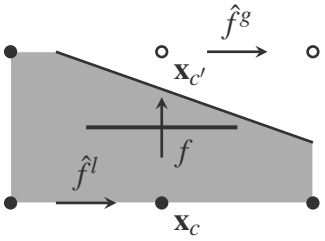

Figure 3: Example Md-GFM gradient stencil for an interface normal face $f \in \mathcal{F}_{I_\eta}$.

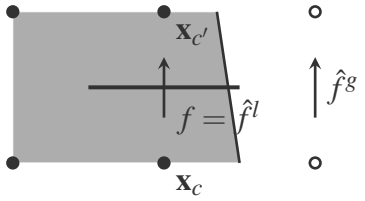

Figure 4: Example Md-GFM gradient stencil for an interface tangential face $f \in \mathcal{F}_{I_\tau}$.

The discretization of the gradient operator for an interface normal face is as follows. We define a jump interpolant J which given $u \in \hat{F}^h$ yields a consistent approximation to the jump of the vector-valued function $\mathbf{u}$

$$J : \hat{F}^h \to F^h \times F^h, \quad u_f \mapsto (Ju)_f \approx [\![\mathbf{u}]\!](\mathbf{x}_f). \tag{18}$$

We choose two faces $\hat{f}^g \in \hat{\mathcal{F}}^g, \hat{f}^l \in \hat{\mathcal{F}}^l$ whose face normals are orthogonal to η_f, from which we define the jump interpolant as

$$(Ju)_f = \eta_f [\![u_f]\!] + \eta_{\hat{f}^g} u^g_{\hat{f}^g} - \eta_{\hat{f}^l} u^l_{\hat{f}^l}, \tag{19}$$

see also Figure 3. Using this jump interpolant we can consistently impose (9)

$$\eta_{i_f} \cdot \left[(Jg)_f - (Ju^*)_f \right] = 0. \tag{20}$$

Combining (19) & (20), and solving for $[\![g_f]\!]$ yields the jump across the face f

$$b^\eta_f = \frac{\eta_{i_f} \cdot (Ju^*)_f}{\alpha_{i_f,f}} - \frac{\alpha_{i_f,\hat{f}^g}}{\alpha_{i_f,f}} g^g_{\hat{f}^g} + \frac{\alpha_{i_f,\hat{f}^l}}{\alpha_{i_f,f}} g^l_{\hat{f}^l}. \tag{21}$$

The faces $\hat{f}^g, \hat{f}^l$ should be chosen such that the evaluation of the interpolant can be done explicitly, hence $\hat{f}^\pi \notin \hat{\mathcal{F}}_{I_\eta}$. Moreover the interpolant should result in a compact stencil and we therefore restrict ourselves to a 6-point stencil for the Md-GFM gradient.

We found that ensuring $\left| \frac{\alpha_{i_f,\hat{f}^\pi}}{\alpha_{i_f,f}} \right| \leq 1$ greatly improves the quality of the Md-GFM operator in time-dependent problems (this requires further investigation). For faces $f \in \mathcal{F}_{I_\eta}$ for which this ratio exceeds 1 we interpret the face as an interface tangential face instead.

For an interface tangential face $f \in \mathcal{F}_{I_\tau}$ we do not impose the gradient jump condition (9). Instead we select two faces $\hat{f}^g, \hat{f}^l$ (one of which coincides with f itself) with the same face normal direction but each in a different phase, which we use for computing the gradient jump. See also Figure 4. This results in the following gradient jump

$$b^\tau_f = \frac{1}{\rho^g} (Gp)_{\hat{f}^g} - \frac{1}{\rho^l} (Gp)_{\hat{f}^l}. \tag{22}$$

Composition of the CCM divergence operator with the aforementioned modifications to the gradient operator defines our Laplace operator. The stencil is no larger than 3×3, and the Laplace operator is no longer self-adjoint but can still be shown to be negative semi-definite with only the constant pressure in the null-space.

4 Validation

Here we consider the validation of the proposed discretization. We first assess the accuracy of the discretized Poisson problem and then consider the more exciting dam-break problem.

4.1 Poisson problem

We compare our proposed method to the Immersed Interface Method (IIM) [3] which sharply imposes jump conditions directly on the Laplacian. The 1d-GFM [4], implemented as described in Section 3.3.2, is also included in the comparison. Whenever the methods 1d-GFM or Md-GFM are referred to in the context of a Laplace operator, the composition with the CCM divergence operator (13) is implied.

We consider the following Poisson problem given by Leveque and Li [3] (therein refered to as 'Problem 3' with $\beta = \rho^{-1}$)

$$\nabla \cdot \left(\frac{1}{\rho} \nabla p \right) = f, \quad \mathbf{x} \in \Omega = (-1,1)^2. \tag{23}$$

The right-hand side f, the Dirichlet boundary conditions, as well as the jump conditions at the interface are such the exact solution is given by

$$p = \begin{cases} \exp(x)\cos(y) & \text{if } \mathbf{x} \in \Omega^l \\ 0 & \text{if } \mathbf{x} \in \Omega^g \end{cases}, \tag{24}$$

where Ω^l is the interior of a circle with radius $\frac{1}{2}$ centered at the origin. Note that p is discontinuous and has a jump in the normal as well as tangential derivative.

4.1.1 Mesh refinement

We let $\rho^l = \rho^g = 1$ and vary the mesh-width as $h = 2/N$ where $N = 10 \times 2^l$ for $l = 1, \ldots, 5$. The resulting L^∞ errors in the pressure are shown in Table 1. As expected, the 1d-GFM is first-order accurate, whereas the Md-GFM is second-order accurate, and of comparable accuracy to the IIM. The main advantage of using the Md-GFM is that the Laplace operator itself follows from the *composition* of a divergence operator and a gradient operator which is required in the context of solving incompressible two-phase problems.

4.1.2 Varying the density ratio

To asses the dependence of the errors on the density ratio we fix the mesh-width $h = 2/80$, and vary the density ratio. The resulting gradient errors are shown in Table 2. We note that the

N	IIM	1d-GFM	Md-GFM
20	4.38×10^{-4}	7.78×10^{-3}	2.67×10^{-3}
40	1.08×10^{-4}	6.48×10^{-3}	6.15×10^{-4}
80	2.78×10^{-5}	6.47×10^{-3}	1.56×10^{-4}
160	7.50×10^{-6}	3.20×10^{-3}	3.36×10^{-5}
320	1.74×10^{-6}	1.49×10^{-3}	9.11×10^{-6}

Table 1: The resulting error $\|p-p^h\|_{L^\infty}$ for the Poisson problem defined by (24). Results for IIM are taken from Leveque and Li [3].

ρ^g/ρ^l	$\|\frac{1}{\rho}\nabla p-\frac{1}{\rho}Gp^h\|_{L^\infty}$
10^6	3.14×10^{-2}
10^3	3.14×10^{-2}
10^0	3.24×10^{-2}
10^{-3}	2.14×10^{-2}
10^{-6}	2.14×10^{-2}

Table 2: Dependence of the scaled gradient error on the density ratio ρ^g/ρ^l for the Md-GFM.

accuracy of the gradient is independent of the density ratio. Hence the proposed method can be used to accurately simulate near the one-phase limit $\rho^g \to 0$.

4.2 A dam-break problem

The proposed discretization has been implemented in our in-house free-surface Navier-Stokes solver ComFLOW. Local and adaptive mesh refinement is used, as detailed in Van der Plas [7]. We validate our model using a smooth version of the classic dam-break problem.

4.2.1 Problem description

The domain is a rectangle of size $20\times12m$ with an elliptic bathymetry of half lengths 18 and $2.8m$ whose center lies in the left-hand side bottom corner. Slip boundary conditions are imposed on the velocity field. The liquid density is given by $\rho^l = 10^3 kg/m^3$, the gas density varies and will always be indicated. Both fluids are initially at rest and separated by the following interface profile

$$y(x) = 7.6 + 3.6\tanh\left(0.36\left(x-12.5\right)\right), \tag{25}$$

which will result in a flip-through impact (FTI) [1] in which the wave trough and crest reach the wall at the same time instance, resulting a violent impact. The gravitational acceleration is set to $g=-9.81m/s^2$ and the surface energy coefficient is that of the combination of water and air at $25^\circ C$: $\sigma = 7.2\times10^{-2}J/m^2$. A static contact angle boundary condition of 90° is imposed on the curvature.

Our base mesh is uniform with $N_x = 80$ and $N_y = 48$ cells in the x- and y-direction respectively. We consider several levels of mesh refinement, where we refine the mesh near the interface using blocks of size 16×16. The refinement level at the interface $l \in \{2,3,4\}$ will always be indicated, the resulting interface mesh-width is given by $h = 2^{-(l+2)}m$.

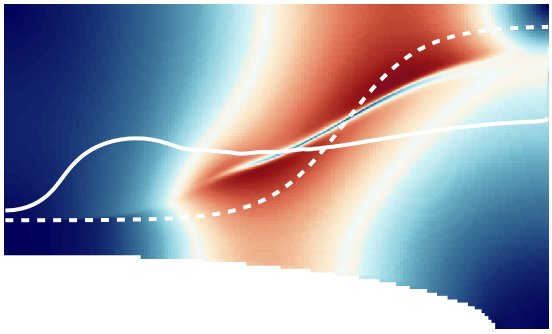

Figure 5: Standard two-phase model. Absolute velocity $|\mathbf{u}|$ at $t = 0.75$. Interface is shown at $t = 0$ & 1.47.

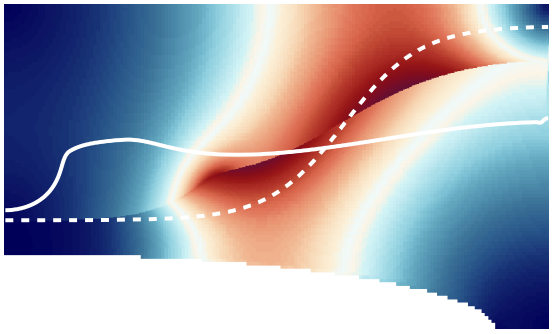

Figure 6: Proposed two-phase model. Absolute velocity $|\mathbf{u}|$ at $t = 0.75$. Interface is shown at $t = 0$ & 1.47.

4.2.2 Comparison to standard two-phase method

Here we demonstrate the efficacy of the proposed model when compared to the standard two-phase model[2]. We let $\rho^g = 1$ and $l = 3$.

In Figures 5 & 6 we show the resulting absolute velocity. We also show the initial interface profile (dashed) and at a later time $t = 1.47$ (solid). Note that the standard two-phase model has a thin region at the interface in which the velocity transitions from gas to liquid. Our proposed model captures this transition in a discontinuity, which allows the breaking wave to develop properly, as seen by the interface profile at $t = 1.47$.

4.2.3 Mesh refinement

We let the gas density be 1 and we consider three levels of refinement $l = 2,3,4$. In Figure 7 we show a close-up of the resulting interface profiles, as well as the tangential velocity jump $[\![u_\tau]\!]$ along the interface. Results by the CADYF code[3][1] are included.

Except for the highest level of refinement, $l = 4$, we observe convergence towards the reference solution. For the highest refinement level, we observe a small fragmentation of the interface at the location where the velocity discontinuity is largest. Whether this is physical, and occurs only at the finest level because it is underresolved at the coarse level, or a numerical artifact, is unclear. The reference solution clearly does not exhibit this behavior, but this could be attributed to numerical damping.

4.2.4 Varying the density ratio

Furthermore we consider the dependence of the solution on the gas density. To this end we fix the refinement level at $l = 3$, and vary the gas density as $\rho^g = 10^{-3}, 1, 3$ and $5 kg/m^3$. For the

[2]The numerical scheme was identical except for the condition $[\![u_\tau]\!] = 0$ and the use of first-order upwind throughout the entire domain. For our proposed model the symmetry-preserving central discretization was adequate.

[3]CADYF is a PSPG-SUPG FEM code which implements the two-phase Navier-Stokes equations using the ALE formulation.

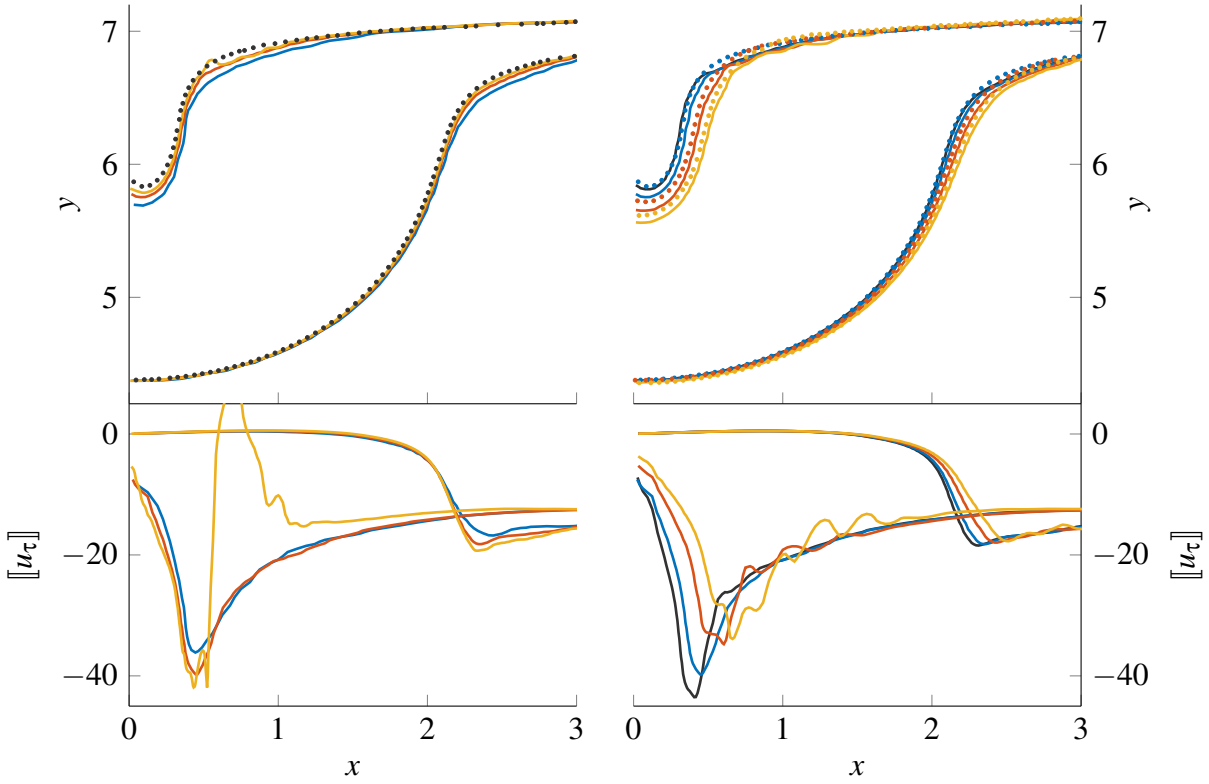

Figure 7: Interface profiles (top) and velocity discontinuity (bottom) for $\rho^g = 1 kg/m^3$ at two time-instances $t = 1.47, 1.67$. Refinement levels are $l = 2$ (blue), 3 (red) and 4 (yellow). Reference solution by CADYF (black markers) [1].

Figure 8: Interface profiles (top) and velocity discontinuity (bottom) for gas densities $\rho^g = 10^{-3}$ (black), 1 (blue), 3 (red) and $5 kg/m^3$ (yellow) at $t = 1.47, 1.67$. The refinement level was $l = 3$. Reference solutions by CADYF (colored markers) [1].

latter three we have a reference solution by CADYF [1].

We find fairly good agreement in terms of the interface profile. The maximum tangential velocity jump increases as the gas density decreases, which may be expected. Moreover, for the larger gas densities, oscillations in the tangential velocity jump can be observed just before impact. This suggests that free surface instabilities are about to develop. The fact that such oscillations are not present for $\rho^g = 10^{-3}$ means that we successfully approach the one-phase limit in which no free surface instabilities due to shearing gas flow are present.

5 Conclusion

We presented a discretization approach for capturing contact discontinuities in two-phase flow. The discretization of the pressure Poisson problem plays a central role since it implicitly couples the phases using a gradient jump condition which corresponds to imposing smoothness of the velocity field *only in the interface normal direction*. A novel combination of our proposed Md-GFM and the CCM was used to achieve this. Using the dam-break problem we then

demonstrated that this approach is able to capture contact discontinuities sharply and accurately, even at high density ratios (demonstrated up to 10^{-6}) close to the one-phase limit.

For the discretization presented in this paper there are several aspects that need further investigation: uniquely defining the Md-GFM jump interpolant to improve the properties of the Laplace operator as well as thorough analysis of the convection scheme near the interface.

The model will be extended with gas compressibility and the effects of viscosity will be included. When modeling viscous flow, the velocity jump condition becomes a closure model for underresolved boundary layers. Eventually we want to use this model to study the effects of free surface instabilities in sloshing of LNG and its vapor.

Acknowledgements

This work is part of the research programme SLING, which is (partly) financed by the Netherlands Organisation for Scientific Research (NWO).

References

[1] Etienne, S., Scolan, Y.-M., and Brosset, L. (2018). Numerical Study of Density Ratio Influence on Global Wave Shapes Before Impact. In *2*, pages 1–11.

[2] Lafeber, W., Brosset, L., and Bogaert, H. (2012). Comparison of Wave Impact Tests at Large and Full Scale : Results from the Sloshel Project. In *Twenty-Second (2012) International Offshore and Polar Engineering Conference*, volume 4, pages 285–299.

[3] Leveque, R. J. and Li, Z. (1994). The Immersed Interface Method for Elliptic Equations with Discontinuous Coefficients and Singular Sources. *SIAM Journal on Numerical Analysis*, 31(4):1019–1044.

[4] Liu, X.-d., Fedkiw, R. P., and Kang, M. (2000). A Boundary Condition Capturing Method for Poisson's Equation on Irregular Domains. *Journal of Computational Physics*, 160:151–178.

[5] Popinet, S. (2009). An accurate adaptive solver for surface-tension-driven interfacial flows. *Journal of Computational Physics*, 228(16):5838–5866.

[6] Udaykumar, H. S., Kan, H.-c., Shyy, W., and Tran-son tay, R. (1997). Multiphase Dynamics in Arbitrary Geometries on Fixed Cartesian Grids. *Journal of Computational Physics*, 137(2):366–405.

[7] Van der Plas, P. (2017). *Local grid refinement for free-surface flow simulations*. PhD thesis, Rijksuniversiteit Groningen.

[8] Verstappen, R. and Veldman, A. E. P. (2003). Symmetry-preserving discretization of turbulent flow. *Journal of Computational Physics*, 187(1):343–368.

[9] Zinjala, H. K. and Banerjee, J. (2015). A Lagrangian-Eulerian Volume-Tracking with Linearity-Preserving Interface Reconstruction. *Numerical Heat Transfer, Part B*, 68:459–478.